Breast Cancer Research

RESEARCH

Open Access

Single-cell landscape of intratumoral heterogeneity and GABA-mediated remodeling of the immune microenvironment in breast cancer metastases

Lina Tang[1*]

Abstract

Background Breast cancer is one of the most prevalent malignant tumors among women, with its metastasis serving as a leading cause of mortality in affected patients. Recent studies have increasingly highlighted the significant role of tumor in nervation in the development and progression of breast cancer; however, the specific underlying mechanisms remain poorly understood.

Methods This study investigated the relationship between tumor immune microenvironment (TIME) cell subpopulations, mediated by neuro-immune mechanisms in metastatic sites of breast cancer, and both disease severity and treatment response. We employed an analysis of single-cell transcriptomics (scRNA-seq) in conjunction with bulk RNA-seq data. The single-cell dataset GSE158399 was obtained from the GEO database, while bulk RNA-seq data from breast cancer patients were retrieved from UCSC Xena. The analysis utilized tools such as Seurat, CellChat, and Monocle, along with a GABA-related gene set.

Results Our results identified 9 major cell types in the metastatic sites of breast cancer, including T cells, B cells, myofibroblasts, epithelial cells, macrophages, endothelial cells, proliferating cells, mature dendritic cells, and mast cells. Notably, the B cell subpopulation B_C2, the $CD4^+$ T cell subpopulation $CD4^+$Tcm, the M2 macrophage subpopulation, and the myofibroblast subpopulation Myo_C2 were associated with the GABA gene set and appeared to play crucial roles in cell differentiation and intercellular communication. The analysis of cell communication revealed that the GABA-mediated TIME model enhanced intercellular signaling, with receptor-ligand pairs such as PTN/MDK-NCL, CXCL12-CXCR4, and APP-CD74 exhibiting significant functional patterns within the samples. Additionally, the bulk RNA-seq data analysis identified the target gene COL1A2, whose expression was significantly correlated with tumor grading and metastatic status, indicating that Stage III patients had higher expression levels than those in Stage I and II, and that the N2 and N3 metastatic groups exhibited higher expression than the N0 group.

*Correspondence:
Lina Tang
tanglina@zzu.edu.cn

Full list of author information is available at the end of the article

© The Author(s) 2026. **Open Access** This article is licensed under a Creative Commons Attribution-NonCommercial-NoDerivatives 4.0 International License, which permits any non-commercial use, sharing, distribution and reproduction in any medium or format, as long as you give appropriate credit to the original author(s) and the source, provide a link to the Creative Commons licence, and indicate if you modified the licensed material. You do not have permission under this licence to share adapted material derived from this article or parts of it. The images or other third party material in this article are included in the article's Creative Commons licence, unless indicated otherwise in a credit line to the material. If material is not included in the article's Creative Commons licence and your intended use is not permitted by statutory regulation or exceeds the permitted use, you will need to obtain permission directly from the copyright holder. To view a copy of this licence, visit http://creativecommons.org/licenses/by-nc-nd/4.0/.

Conclusion This study suggests that GABA may reshape the TIME through the modulation of the neuro-immune axis, offering new insights for prognostic assessments and the development of therapeutic targets in breast cancer metastasis.

Keywords Breast cancer, Immune microenvironment, Tumor innervation, GABA, Metastasis, Single-cell analysis

Introduction

Breast cancer is one of the leading causes of cancer-related mortality among women worldwide, with its high mortality rate closely linked to the development of metastases and treatment resistance [1]. The tumor microenvironment (TME) plays a crucial role at various stages of tumor development, metastasis, immune evasion, and treatment response [2]. The heterogeneity of the TME has been recognized as a significant factor driving tumor progression and metastasis. Variability in immune cell subtypes and genetic characteristics within the TME is essential for both tumor advancement and sustained treatment efficacy [3]. The immunosuppressive nature of TIME is a common characteristic of cancer and a key contributor to treatment failure [4, 5]. While previous research has primarily concentrated on the interactions between tumor cells and immune cells, such as T cells and macrophages, emerging evidence suggests that the interplay between the nervous system and the immune system—termed the neuro-immune axis—may reshape the TIME through neurotransmitter signaling, consequently influencing tumor progression [6–8].

γ-aminobutyric acid (GABA), the primary inhibitory neurotransmitter in the central nervous system, is aberrantly expressed in peripheral tumor tissues and is closely linked to the regulation of immune cell functions [9]. For instance, GABA has been shown to suppress intratumoral infiltration of $CD8^+$ T cells and promote tumor cell proliferation through the activation of β-catenin [10]. Additionally, it has been reported that GABA derived from B cells inhibits the cytotoxic function of $CD8^+$ T cells by facilitating the differentiation of monocyte into anti-inflammatory $IL\text{-}10^+$ macrophages [11]. Dong et al. demonstrated that tumor cell-derived GABA promotes the progression of lung cancer by influencing macrophage polarization within the TME. Specifically, GABA prevents macrophages from polarizing towards the M1 phenotype, while promoting M2 polarization [12]. However, the specific targets of GABA in breast cancer metastases —such as particular immune cell subpopulations—its regulatory networks, and their associations with clinical outcomes including metastatic risk and treatment response, remain poorly understood. Furthermore, there is a lack of studies investigating the spatiotemporal dynamics of neuro-immune interactions at single-cell resolution, as well as the molecular mechanisms involved, utilizing integrated multi-omics data.

In this study, we employed scRNA-seq and bulk RNA data to identify specific neuro-immune-related IME cell subtypes within breast cancer. We further investigated the clinical and biological characteristics of these subpopulations, as well as their interactions with other cell types. Additionally, we analyzed the differential therapeutic responses among these subpopulations. Initially, we utilized the non-negative matrix factorization (NMF) algorithm to identify GABA-related cell clusters within the tumor microenvironment. We then examined temporal trajectories, intercellular communication, and regulatory networks to elucidate the distinctions among various breast cancer cell clusters. Moreover, functional enrichment analyses based on HALLMARK and REACTOME pathways were conducted to uncover the functions of these different breast cancer subtypes. In summary, our comprehensive single cell-based exploration reveals for the first time that GABA-associated genes may influence communication between tumor cells and TIME cells, thereby promoting breast cancer development.

Materials and methods

Data collection and processing

Single-cell RNA sequencing (scRNA-seq) data GSE158399 were obtained from the Gene Expression Omnibus (GEO) database, encompassing three datasets: GSM4798908 (primary breast cancer), GSM4798909 (metastasis-positive lymph node, PLN), and GSM4798910 (metastasis-negative lymph node, NLN). Compare according to the following groups : primary breast vs. lymph node (site/context comparison); PLN vs. NLN (within-lymph-node, metastasis-positive vs. metastasis-negative comparison).

Additionally, bulk RNA-seq data from 1203 primary breast cancer samples were sourced from the UCSC Xena database (https://xena.ucsc.edu/), ensuring the exclusion of patients lacking survival time data.

GABA-related gene set and definition of GABA-high subpopulations.

A set of 1417 GABA-related genes was compiled by searching the GeneCards database (https://www.genecards.org/) with the keyword “GABA” (access date: 2025-02-15; Supplementary Table 1). To identify GABA-high cell subpopulations, we calculated the average expression level of these GABA-related genes in each cell subpopulation using the AverageExpression function in Seurat. Within each major cell lineage (B cells, T cells, macrophages, myofibroblasts), the subpopulation exhibiting

the highest average expression was designated as the predominant GABA-associated subtype.

ScRNA-seq data quality control and dimensionality reduction

For the processing of single-cell datasets, the R (4.1.2) package "Seurat (4.2.1)" was utilized to construct Seurat objects. Quality control was performed by filtering out cells with fewer than 200 or more than 5000 features and excluding cells with fewer than 200 counts and cells with mitochondrial gene percentage exceeding 20%. Additionally, cells with total UMI count (nCount_RNA) greater than 8000 were removed.

Data normalization was accomplished using the NormalizeData function, followed by the identification of the top 3000 highly variable genes through the "vst" method via the FindVariableFeatures function. The dataset was further normalized using the ScaleData function. Principal Component Analysis (PCA) was executed with the RunPCA function, and the number of principal components (PCs) to be retained was determined through visual inspection with the ElbowPlot function; 20 PCs were selected for downstream analysis.

Subsequently, UAMP visualization was performed using the RunUMAP function, setting n.neighbors to 30 and dims to 1:30. To account for batch effects across different samples, the Harmony algorithm was applied. This algorithm adjusts the expression profiles of cells to harmonize data from various samples, mitigating batch effects that could confound downstream analyses. Batch correction was conducted using the R package Harmony with default parameters (max.iter.harmony = 30, reduction = "pca").

Following batch correction, a shared nearest neighbor (SNN) graph was constructed with the first 20 principal components using the FindNeighbors function. Cell clustering was performed with the FindClusters function, and after testing multiple resolutions (0.01–1), a resolution of 0.2 was selected for final cluster assignment. Cluster identity was further annotated using classic marker gene references from literature.

Pseudotime trajectory analysis of cell subpopulations

The R package "monocle" (version 2.22.0) was utilized to perform time-series analysis on distinct cell subpopulation. Initially, a CellDataSet (CDS) object was created using the newCellDataSet function, followed by the application of the estimateSizeFactors and estimateDispersions functions to compute size factors and dispersions for the dataset. Feature genes were selected and organized based on the high-variable genes identified using the FindVariableFeatures function, and the setOrderingFilter was applied to prioritize these genes for further analysis. Subsequently, dimensionality reduction was conducted using the reduceDimension function, employing the reverse graph embedding (DDRTree) algorithm. Finally, a cell trajectory map was constructed based on pseudotime and the cell subpopulation groups, and the pseudo-time expression of GABA-related genes was visualized using the plot_pseudotime_heatmap function.

Communication analysis of cell subpopulations

Cell communication refers to the process through which cells exchange information via signal transmission and interaction. The R package "CellChat" was used to simulate cell communication. The createCellChat function was utilized to generate a CellChat object, while the identifyoverExpressedGenes function was applied to identify highly expressed genes, using default parameters for the analysis. Additionally, the identifyoverExpressedInteractions function was employed to investigate overexpressed ligand-receptor interaction pairs within the CellChatDB. The computeCommunProb function was then used to calculate the communication probability (intensity) between various cell subpopulations.

SCENIC analysis

We conducted a gene regulatory network analysis for each cell subtype using the pySCENIC software, with the normalized expression matrix from Seurat serving as the input. The files hg19-500 bp-upstream-7species.mc9nr.feather and hg19-tss-centered-10 kb-7species.mc9nr.feather were ontained from the RcisTarget database. Initially, we identified the co-expression modules involving transcription factors and their potential target genes. Sunsequently, we inferred direct target genes based on the significantly enriched potential targets associated with the corresponding transcription factors. Lastly, we estimated the regulatory subunit activity score for each individual cell using the area under the ROC curve and compared the differences in regulatory subunit activity scores among the various subtypes.

External validation using an independent scRNA-seq cohort

To validate the observed trends, we analyzed an independent scRNA-seq dataset GSE180286, which includes 5 primary breast cancer samples and 10 lymph node metastasis samples. Data were processed using the same pipeline and parameters as for GSE158399. Cell types were annotated using the same marker genes, and GABA-related gene expression patterns were compared.

Results

The single-cell landscape of breast cancer metastatic tumor cells

Quality control was performed on the single-cell data (GSE158399), resulting in the retention of 30,529 cells

for subsequent analysis (Figure S1A). We identified 3000 highly variable genes, including IGHG1, IGHG4, IGHG2, IGLV2 – 14, among others (Figure S1B). The top 30 principal components (PCs) were selected for further analysis (Figure S1C), and Harmony was utilized to eliminate batch effects among the samples (Figure S1D). Cell clustering was conducted using the FindClusters function with a resolution of 0.2, which led to the identification of 13 distinct cell clusters (Figure S1E). These subtypes were annotated based on previous studies and the FindAllMarkers function in Seurat, resulting in the identification of 9 different cell subtypes: T cells (11765 cells), B cells (8340 cells), myofibroblasts (5131 cells), epithelial cells (2555 cells), macrophages (1477 cells), endothelial cells (523 cells), proliferating cells (477 cells), mature dendritic cells (210 cells), and mast cells (72 cells) (Fig. 1A). The marker genes for all cell types are presented in Figure S1F. Additionally, the differentially expressed genes (DEGs) and corresponding functional pathway enrichment results for each cell type are illustrated in Figure S2. Cellular communication analysis revealed a diverse range

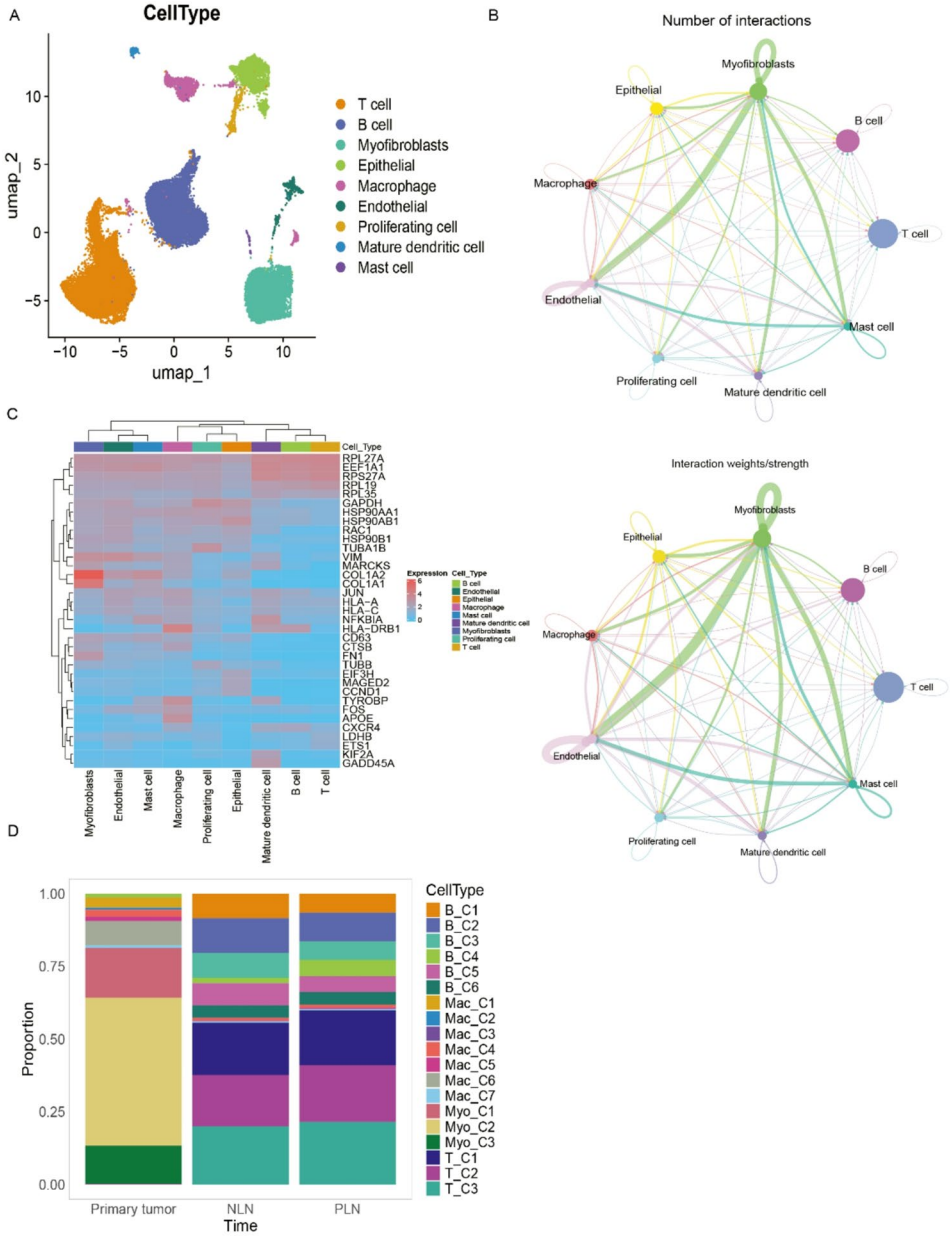

Fig. 1 The landscape of cell subtypes. **A** UMAP plots of 9 distinct cell subtypes in breast cancer. **B** Circos plots showing the number and strength of the communication interactions across 9 cell types. **C** Heatmap of GABA-related gene expression in distinct cell subtypes. **D** Classification of GABA-mediated TIME cell subpopulations by the NMF algorithm in the scRNA-seq data

of interaction numbers and strengths among these cellular subtypes (Fig. 1B).

Of note, with only one sample per condition (primary, NLN, PLN), statistical comparisons of cell proportions are not feasible; all reported differences are descriptive and should be interpreted as hypothesis-generating. Potential influences of tissue dissociation or composition effects cannot be excluded.

Furthermore, we identified 1417 GABA-related genes from the MSigDB and iUUCD databases and assessed their differential expression levels among the 9 cell subtypes within the breast cancer tissue, as shown in Fig. 1C. To further delineate GABA-mediated subsets of the TIME cells, we performed additional subpopulation analysis for the main TIME cell types based on the GABA-related gene sets and employed the NFM clustering method. As illustrated in Fig. 1D, B cells were classified into 6 distinct subpopulations, while T cells were re-clustered into 3 distinct subpopulations. Macrophages were divided into 7 distinct subpopulations, and myofibroblasts revealed 3 stable clusters. Notably, compared to the primary tumor sample, lymph node samples (both NLN and PLN) showed decreased relative proportions of Mac_C1, Mac_C6, Myo_C1, Myo_C2, and Myo_C3. Conversely, the relative proportions of B_C1, B_C2, B_C3, B_C5, B_C6, T_C1, T_C2, and T_C3 increased in lymph node samples compared to the primary sample.

To assess the generalizability of our findings, we analyzed the independent scRNA-seq dataset GSE180286 (5 primary, 10 lymph node metastases). After quality control and clustering, we identified major cell types including T cells, B cells, myofibroblasts, epithelial cells, macrophages, endothelial cells, and proliferating cells (Figure S3A). Consistent with our main dataset, lymph node samples showed increased proportions of B cells and T cells and decreased proportions of myofibroblasts compared to primary samples (Figure S3B). The average expression of GABA-related genes across cell types exhibited a similar pattern, and heatmap of the top 10 GABA-related genes per cell type also revealed consistent enrichment (Figure S3C). These results support the robustness of our observations and suggest that GABA-associated cell type distributions are conserved across independent cohorts.

GABA-mediated B cell subpopulations in metastatic breast cancer

A total of 8340 B cells were obtained from scRNA-seq data in breast cancer. To further investigate the differentiation trajectory of B cells in vivo, we identified cell subpopulations based on marker genes for pseudotime analysis, presenting the pseudotime scatterplot of B cells. Pseudotime trajectories of GABA-mediated B cell subpopulations were determined using the NMF algorithm. In this analysis, dark blue indicates earlier differentiation stages, while light blue represents later stages. We observed a continuum of cell states progressing from state 1 to states 2 and 3. Notably, B_C4 was predominantly localized in the terminal state compared to the other 5 subpopulations (B_C1, B_C2, B_C3, B_C5, and B_C6). Conversely, B_C3 was primarily situated at the beginning of the trajectory, whereas B_C1, B_C2, B_C5, and B_C6 exhibited similar trajectories and were evenly distributed (Fig. 2A). Subsequently, we estimated the expression levels of GABA-related genes across the 6 B cell subpopulations. As depicted in Fig. 2B, the highest expression levels of GABA-related genes were found in B_C2, indicting that B_C2 may be the predominant cell type associated with GABA-related gene sets. Compositional analysis revealed that compared to the primary tumor sample, lymph node samples (both NLN and PLN) showed increased percentages of B_C1, B_C2, B_C3, B_C5 and B_C6, and a decreased percentage of B_C4 (Fig. 2C). To further explore branch-dependent genes across the three states, we conducted branched expression analysis modeling (BEAM). This analysis identified a total of 105 genes that may regulate the differentiation process from state 1 (pre-branch) to state 2 (cell fate 1) and state 3 (cell fate 2) (Fig. 2D).

SCENIC analysis was employed to detect differential transcription factors (TFs) activity among various B cell subpopulations. In B_C4, the enriched TFs identified included XBP1, XBP1 extended, JUN, FOS-extended, JUN-extended, FOST, MEF2A-extended, JUND-extended, JUNB- extended, and JUND (Figure S4A). To further explore the correlation between GABA-mediated B cell subpopulations and specific biological pathways, we conducted HALLMARK enrichment analysis to illustrate enrichment scores for each subpopulation. Notably, B_C4 was associated with several pathways, including TNFA signaling via NF-κB, epithelial mesenchymal transition, hypoxia, UV response UP, apoptosis, estrogen response late, estrogen response early, inflammatory response, IL6-JAK-STAT3 signaling, unfolded protein response, and p53 pathway (Figure S4B).

Additionally, we performed Reactome pathway enrichment analysis, which revealed distinct pathway characteristics for the 6 B cell subpopulations. The results indicated that these subpopulations were primarily enriched in pathways related to transmission across chemical synapses, diseases of signal transduction by growth factor receptors and second messengers, signaling by interleukins, and neuronal system pathways, such as interleukin-4 and interleukin-13 signaling, signaling by NTRKs, autophagy, platelet activation, signaling and aggregation, and macroautophagy (Figure S5).

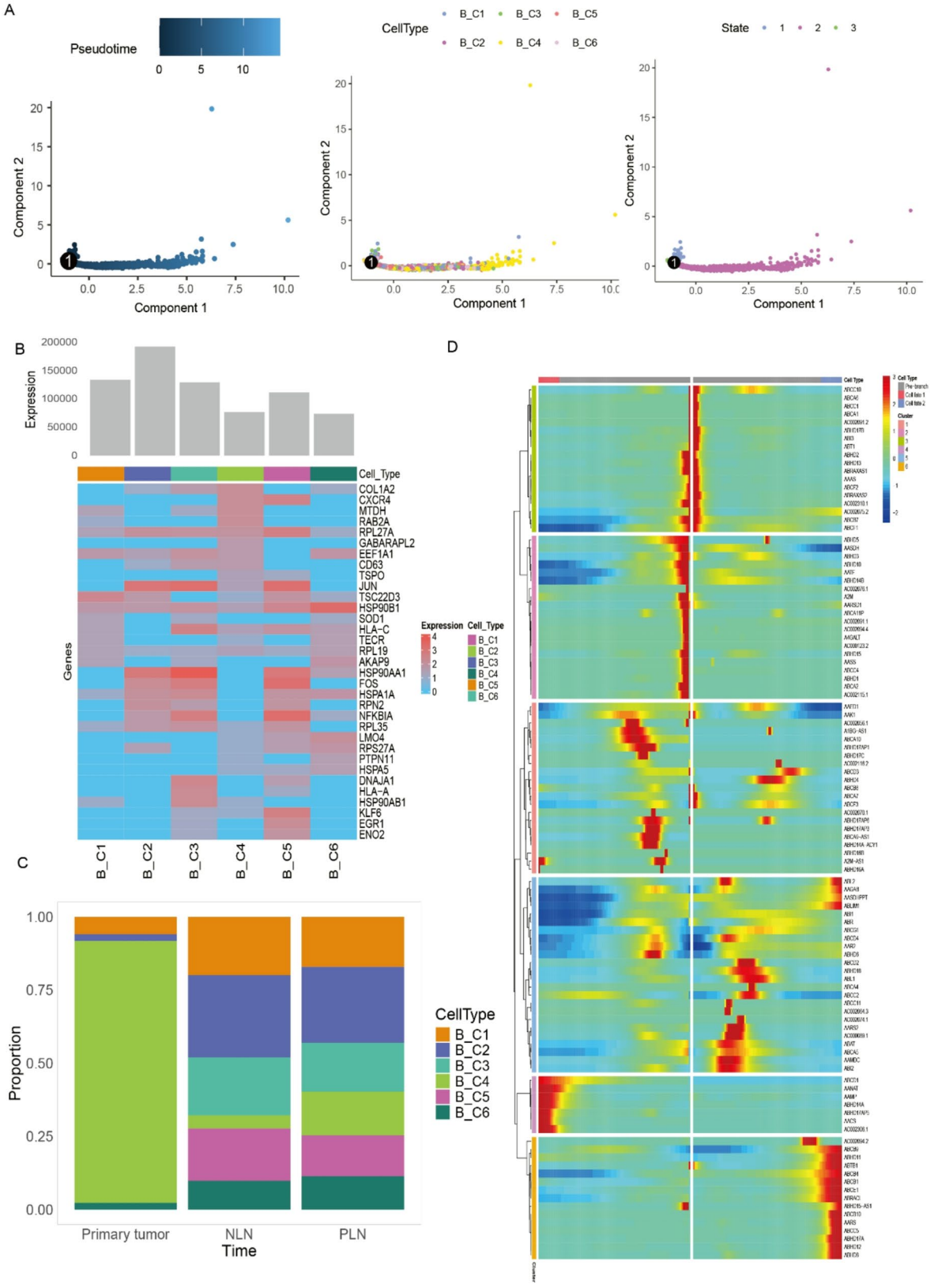

Fig. 2 GABA-mediated B cell subpopulations in breast cancer. **A** Developmental pseudotime and cell state distribution of B cell subpopulations based on the Monocle algorithm in breast cancer. **B** The expression of GABA-related genes across distinct subpopulations. **C** Proportions of 6 subpopulations in each group. **D** BEAM analysis of the differentially expressed genes along pseudo-time across the trajectory

GABA-mediated T cell subpopulations in metastatic breast cancer

T cells constituted a significant proportion of cell types exhibiting notable changes in metastatic samples. We identified 3 subpopulations for pseudotime analysis, with the pseudotime scatterplot of T cells presented in Fig. 3A. Our analysis revealed that the 3 subpopulations displayed similar trajectories and were evenly distributed, effectively a single continuous trajectory, suggesting that the role of GABA is to regulate activity rather than induce reprogramming. We assessed the expression levels of GABA-related genes across the 3 T cell subpopulations, finding the highest expression in $CD4^+$ Tcm, indicating that $CD4^+$ Tcm may be the predominant cell subtype associated with GABA-related gene sets (Fig. 3B). Notably, compared to the primary sample, lymph node samples (NLN and PLN) showed decreased proportions of CD4 + Tcm and CD4 + Tprol and an increased proportion of CD8 + T cells (Fig. 3C). To further investigate branch-dependent genes across the three states, we conducted BEAM analysis, which identified a total of 105 genes potentially regulating the differentiation process from pre-branch to cell fate 1 and cell fate 2 (Fig. 3D). CD4 + Tprol cells were notably enriched in KDM5A, CEBPZ-extended, ZNF91-extended, and HDAC2-extended (Figure S6A). The distinct HALLARK pathways and Reactome terms enriched in the 3 T cell subpopulations are illustrated in Figure S6B and Figure S7, respectively. $CD8^+$ T cells were significantly enriched in KARS signaling DN, while $CD4^+$ Tprol cells were enriched in pathways related to hypoxia, G2M checkpoint, and protein secretion.

GABA-mediated macrophage subpopulations in metastatic breast cancer

Macrophages are the most prevalent infiltrating immune cells in breast cancer and exhibit both anti-tumor and pro-tumor functions. An unsupervised analysis of macrophage subpopulations has identified 2 stable clusters, each characterized by distinct signature genes. The M1 and M2 subpopulations were subsequently analyzed using pseudotime analysis to investigate differentiation trajectories of macrophages in vivo. The pseudotime trajectories of GABA-mediated macrophage subpopulations were determined using the NMF algorithm, revealing a continuum of cell states ranging from state 1 to states 2 and 3 (Fig. 4A). Notably, the expression levels of GABA-related genes were significantly higher in M2 macrophages compared to M1, indicating that M2 is the predominant cell subtype associated with GABA-related gene sets (Fig. 4B). Among these genes, HLA-DRB1, APOE, and TYRPBP were highly expressed in M2 cells, while M1 cells exhibited high expression levels of FOS and RPS27A (Fig. 4B). Compositional analysis revealed that compared to the primary sample, lymph node samples (NLN and PLN) showed an increased percentage of M1 macrophages and a decreased percentage of M2 macrophages (Fig. 4C). The BEAM analysis identified a total of 103 genes that may regulate the differentiation process from pre-branch to cell fate 1 and 2 (Fig. 4D). Furthermore, SCENIC analysis indicated higher TFs activities of BACH1, TAF7-extended, IRF7-extended, EHF-extended, MAZ-extended, ELF3-extended, TAF1-extended, TAF1, JUND-extended, and SIN3A-extended in M1 cells, while NR1H3-extended, NR1H3, MIFT-extended, STAT1-extended, SPI1-extended, SPI1, EGFR-extended, ELF2-extended, MAFB, and MAFB-extended showed higher activities in M2 cells (Figure S8A). GSVA revealed that M1 cells were enriched in pathways related to spermatogenesis and estrogen response early, whereas M2 cells were enriched in pathways associated with coagulation, complement, angiogenesis, and cholesterol homeostasis (Figure S8 B). The Reactome analysis data for M1 and M2 cells are presented in Figure S9.

GABA-mediated myofibroblast subpopulations in metastatic breast cancer

A total of 5131 myofibroblasts were identified from scRNA-seq data in breast cancer, with these cells predominantly detected in primary samples. This finding suggests that myofibroblasts are predominantly detected in primary samples, with reduced detection in lymph node samples, potentially reflecting changes in cellular composition or phenotypic plasticity across tissue contexts. To further investigate the dynamics of myofibroblast subpopulations, we performed pseudotime analysis. This analysis revealed a continuum of cell states characterized by two distinct trajectories, originating from a common state (state 1) and diverging into states 2, 3, 4, and 5. It was observed that the majority of the Myo_C1 subpopulation was concentrated in one trajectory branch, culminating in a terminal state. In contrast, Myo_C2 was primarily located at the beginning of the trajectory (Fig. 5A). The expression levels of GABA-related genes were highest in Myo_C2 cells compared to Myo_C1 and Myo_C3, indicating that Myo_C2 is the predominant cell subtype associated with GABA-related gene sets (Fig. 5B). Proportional analysis indicated that myofibroblasts were exclusively detected in primary tumor samples, with Myo_C2 accounting for the largest proportion among the 3 subpopulations (Fig. 5C). To investigate branch-dependent genes across the 5 states, we conducted BEAM analysis and identified a total of 72 genes that may regulate the differentiation process from pre-branch to cell fate 1and 2 (Fig. 5D). Additionally, we analyzed TFs activity in the 3 distinct myofibroblast subpopulations. As depicted in Figure S10A, Myo_C1 exhibited significantly higher TF activity in ZNF281-extended,

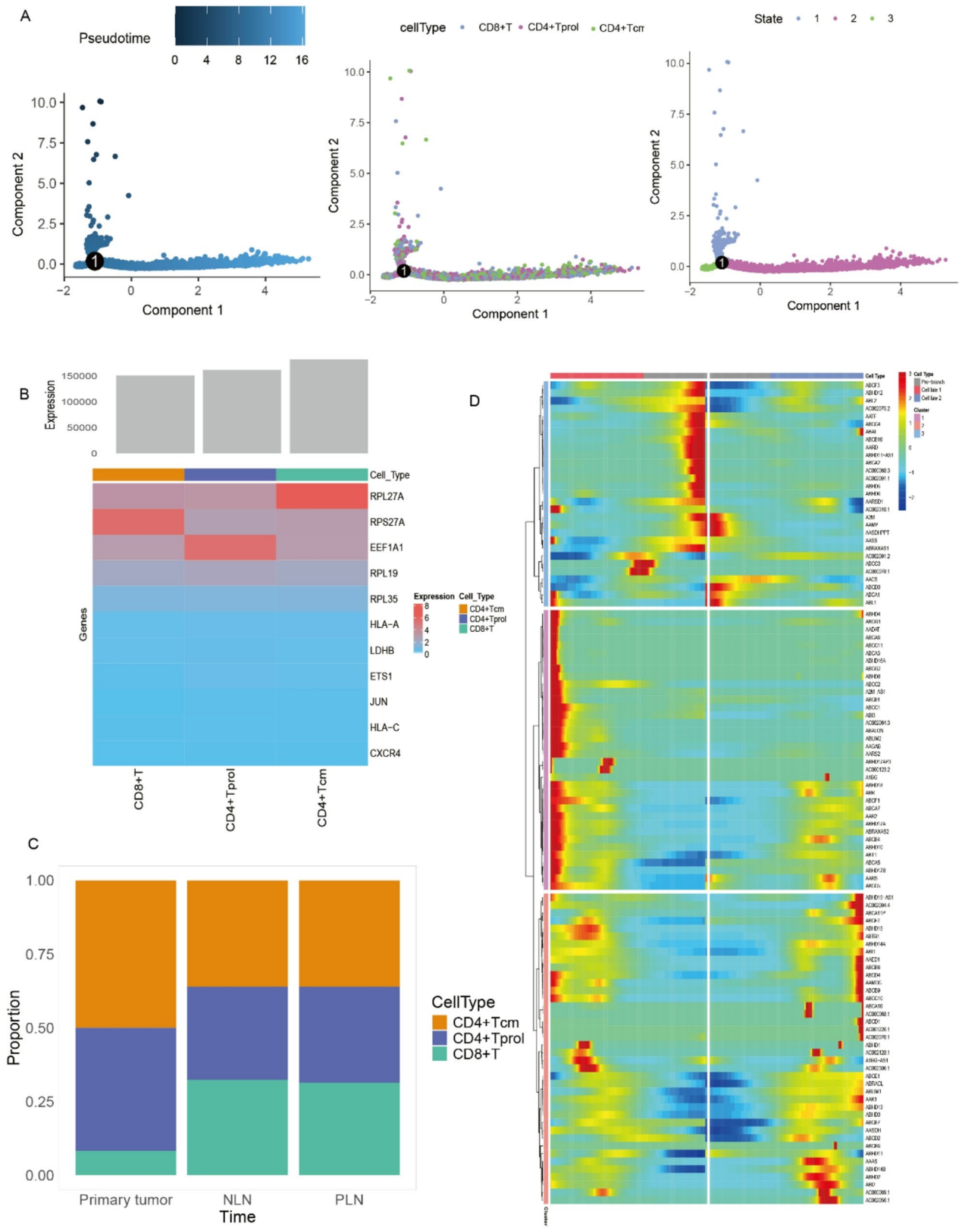

Fig. 3 GABA-mediated T cell subpopulations in breast cancer. **A** Developmental pseudotime and cell state distribution of T cell subpopulations based on the Monocle algorithm in breast cancer. **B** The expression of GABA-related genes across distinct subpopulations. **C** Proportions of 3 subpopulations in each group. **D** BEAM analysis identifying key transition node DEGs along pseudo-time across the trajectory. Heatmaps displaying the top 10 genes with significant changes before and after

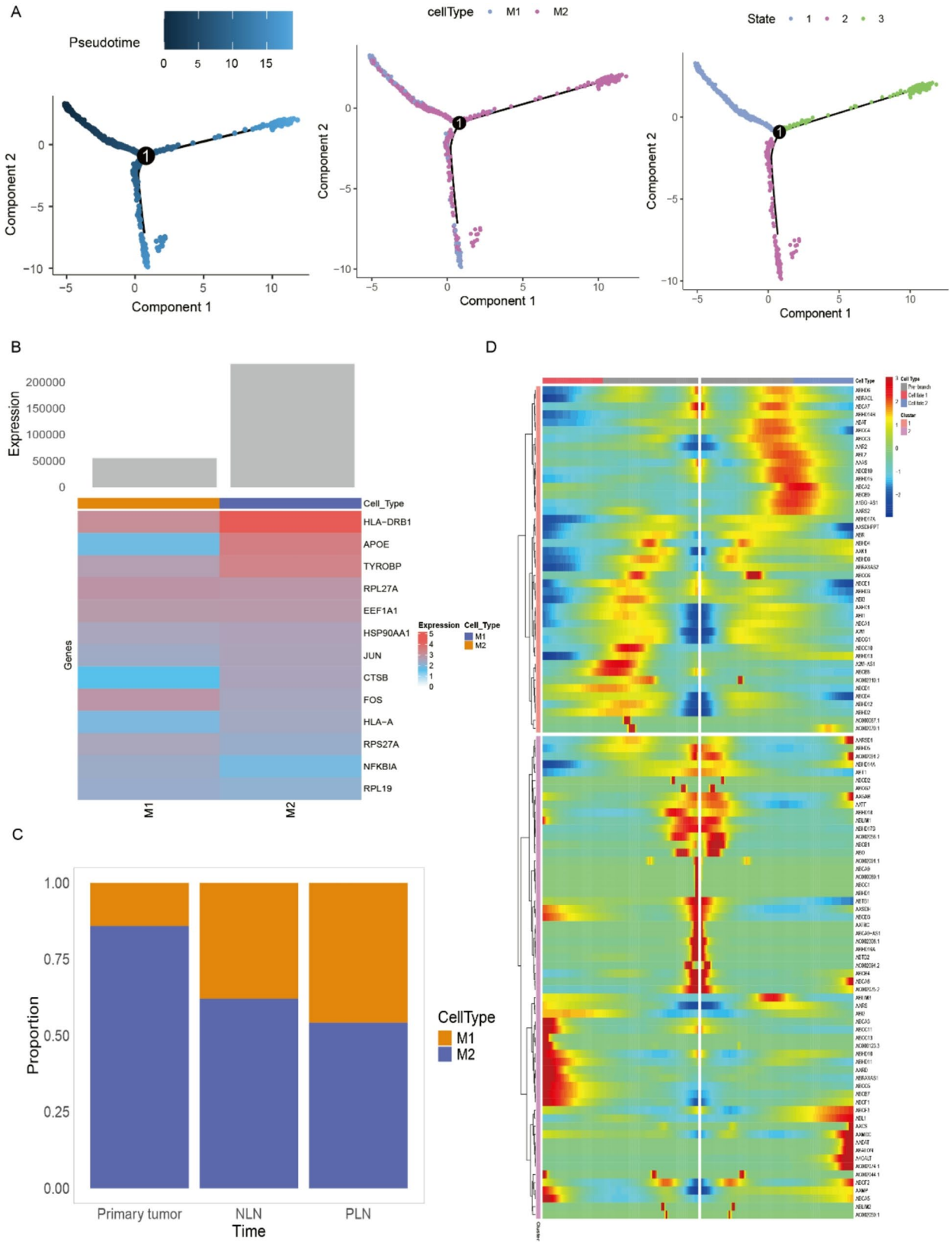

Fig. 4 GABA-mediated macrophage subpopulations in breast cancer. **A** Developmental pseudotime and cell state distribution of macrophage subpopulations based on the Monocle algorithm in breast cancer. **B** The expression of GABA-related genes across distinct subpopulations. **C** Proportions of 2 subpopulations in each group. **D** BEAM analysis identifying key transition node DEGs along pseudo-time across the trajectory. Heatmaps displaying the top 10 genes with significant changes before and after

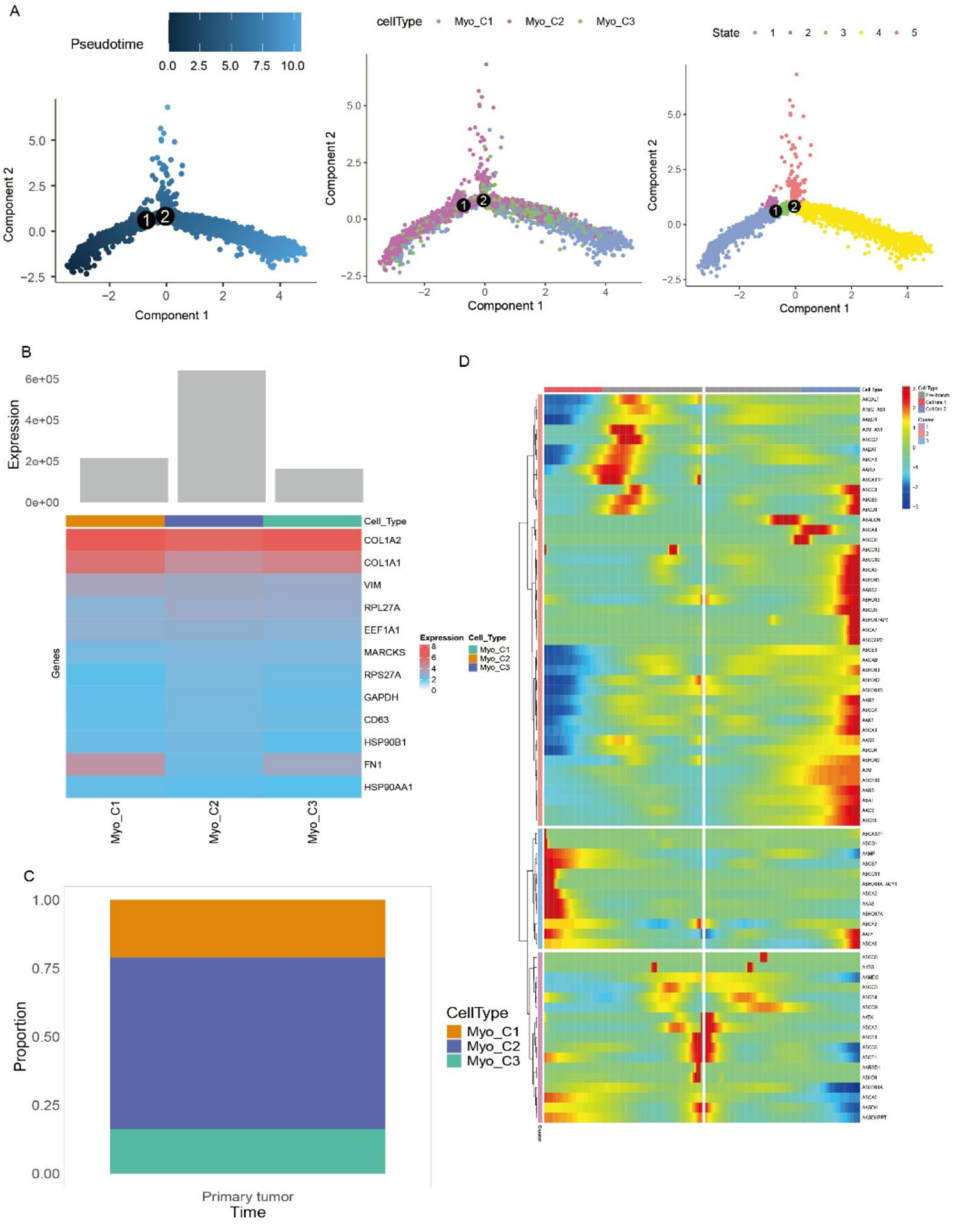

Fig. 5 GABA-mediated myofibroblast subpopulations in breast cancer. **A** Developmental pseudotime and cell state distribution of myofibroblast cell subpopulations based on the Monocle algorithm in breast cancer. **B** The expression of GABA-related genes across distinct subpopulations. **C** Proportions of 3 subpopulations in each group. **D** BEAM analysis identifying key transition node DEGs along pseudo-time across the trajectory. Heatmaps displaying the top 10 genes with significant changes before and after

TRIM28-extended, TAF1-extended, ZMIZ1-extended, FOXN3-extended, SP1-extended, ETV6-extended, EP300-extended, TCF4-extended, KLF2-extended, CREB3L1, CREB3L1-extended, and CREB3. Myo_C2 showed elevated TF activity in GTF2F1, MXI1-extended, ETV1-extended, IRF1-extended, SMARCC2-extended, THAP1-extended, UBTF-extended, UQCRB, CDH2-extended, and CDH2, while Myo_C3 had higher TF activity in ETS1, XBP1-extended, ETS1-extended, XBP1, and ATF6-extended. The HALLMARK enrichment analysis revealed that Myo_C1 was significantly enriched in pathways related to angiogenesis, myogenesis, epithelial mesenchymal transition, apical junction, coagulation, Hedgehog signaling, WNT signaling, mitotic spindle, and IL2-STAT5 signaling. In contrast, Myo_C2 was enriched in pathways associated with oxidative phosphorylation, reactive oxygen species pathway, MYC targets V1, DNA repair, adipogenesis, fatty acid metabolism, peroxisome, p53 pathway, allograft rejection, MYC targets V2, and interferon-α response (Figure S10B). The Reactome analysis data of the 3 subpopulations are shown in Figure S11.

GABA-mediated TIME patterns enhance intercellular communication networks

In the tumor microenvironment, cell–cell interactions play crucial roles in disease progression. Analyzing cell communication can reveal the signaling mechanisms between different cell subpopulations, clarifying the active signaling pathways involved in intercellular interactions. This understanding is essential for clarifying cell-to-cell interactions and uncovering complex biological processes. We employed CellChat analysis to systematically assess the intricate cellular interactions within breast cancer samples and to explore highly correlated ligand-receptor communication networks. Intercellular interactions were predicted based on specific protein complexes, resulting in weighted networks that depict the number and strength of interactions across all cell types. Signal transmission patterns showed that My0_C1 cells acted as the primary signaling hub, followed by My0_C2 and My0_C3 cells (Fig. 6A and B). An analysis of outgoing signals revealed that My0_C1 cells significantly contributed to outgoing signals across various cell subtypes, with My0_C2 and My0_C3 following in contribution (Fig. 6C upper). Subsequently, we classified cell types and their associated signaling pathways using the "NMF" package (Fig. 6D upper). By analyzing the Cophenetic and Silhouette indices of outgoing and incoming signaling, we categorized outgoing cell patterns into 2 distinct groups based on these metrics: Pattern 1 (comprising Myo_1, My0_C2, and My0_C3) and Pattern 2 (including M1 and M2). The outgoing communication patterns were further divided into 2 types. The primary contributors for Pattern 1 included CXCL, FGF, periostin, THBS, collagen, PTN, APP, NEGR, MK, FN1, CD99, annexin, and CADM. In contrast, the major contributors for Pattern 2 were SPP1 and complement (Fig. 6E upper). Following this analysis, we applied a similar approach to incoming signals. We observed that Myo_1 cells were the primary recipients of incoming signals, followed by Myo_C2 and Myo_C3 cells (Fig. 6C lower). The cell types and signaling pathways were categorized into 2 distinct patterns: Pattern 1, which included Myo_1, Myo_C2, and Myo_C3 cells, and Pattern 2, which comprised T_C1, T_C2, T_C3, M1, M2, B_C1, B_C2, B_C3, B_C4, B_C5, and B_C6 (Fig. 6D lower). In communication Pattern 1, the most influential factors included FGF, NEGR, periostin, SPP1, FN1, collagen, THBS, CD99, CADM, MK, and PTN. The primary contributors for Pattern 2 were complement, annexin, APP, and CXCL (Fig. 6E lower) .

The analysis outlined above has elucidated important signaling pathways between cells. Our focus was on investigating the signaling communication between myofibroblasts and macrophages due to the critical role myofibroblasts play in mediating output signals in breast cancer cells. The significant ligand-receptor pairs involved in these signaling pathways are illustrated in Fig. 6F. Notably, the most critical ligand-receptor pairs between myofibroblasts and T and B cells included PTN/MDK-NCL, CXCL12-CXCR4, and APP-CD74. The primary ligand-receptor pair between myofibroblasts and macrophages was identified as ANXA1-FPR1. Among various subclusters of myofibroblasts, the most significant ligand-receptor pairs were FN1/COL1A1/COL1A2-SDC1 and CD99-CD99. Subsequently, we selected the PTN/MDK signaling pathway for further investigation. Pathway analysis revealed that for PTN, Myo_ C1, Myo_ C2 and Myo_ C3 cells served as the main signal emitters, while Myo_ C1 cells were the primary receivers, a process regulated by multiple cell types. For MDK, Myo_ C2 and Myo_ C3 cells again functioned as the primary signal emitters, with Myo_ C1 cells as the main receivers, also regulated by multiple cell types (Fig. 6G). Among these interactions, the PTN/MDK-NCL receptor-ligand pair exhibited the greatest contribution to signaling dynamics (Fig. 6H). Overall, these results highlight the complex receptor–ligand interaction networks and cellular communication within the TIME.

The correlation between GABA-mediated TIME pattern with disease severity and treatment response in metastatic breast cancer

We obtained bulk RNA-seq datasets comprising 1203 samples from TCGA. Through this analysis, we identified distinct sets of differentially expressed genes (DEGs) between 1091 tumor samples and 112 normal samples, resulting in a total of 9554 DEGs (with a threshold of $|\log FC|<1.5$ and an adjusted $p<0.05$). Subsequently, we intersected the 9554 DEGs with those identified in the BEAM analysis of single-cell types (Fig. 7A) and the GABA gene set, which yielded a single gene of interest, COL1A2 (Fig. 7B). Then we explored the relationship between COL1A2 expression and clinical pathological characteristics. The results showed a significant correlation between COL1A2 levels and tumor progression, with notable differences observed across various stage levels (Fig. 7C) and N categories (N0 vs N1–3) (Fig. 7D).

Discussion

Cancer continues to pose a significant health challenge globally, with its progression driven by the complex interactions within the tumor microenvironment (TME), which often lead to treatment resistance. The TME is a multifaceted ecosystem that includes fibroblasts, tumor cells, endothelial cells, immune cells, extracellular matrix (ECM), and various secreted factors [13, 14]. Notably, the neural components of the TME, which play a critical role, are frequently overlooked [15]. Nerve endings extend into the TME and interact with leukocytes to regulate tumor cell growth, invasion, and metastasis [16, 17]. In

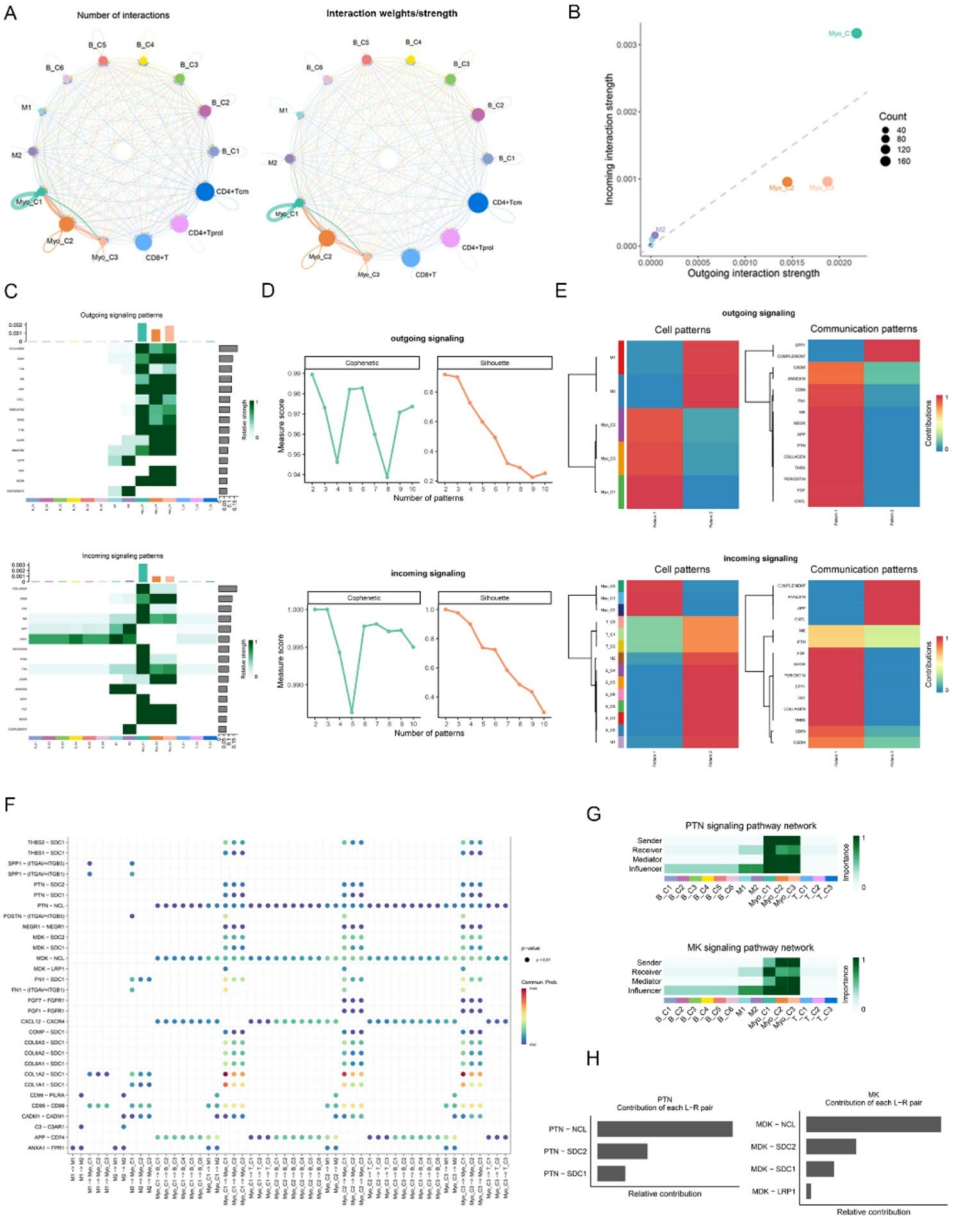

Fig. 6 GABA-mediated myofibroblast subpopulations in breast cancer. **A** Circular plot showing the number and strength of interactions among distinct cell subpopulations in breast cancer. **B** Scatter plot showing the incoming and outgoing signal strength of cell subtypes, illustrating the roles of each subtype in the signaling network. **C** Heatmap displaying the outgoing and incoming signal strength of different cell types. **D-E** Based on Cophenetic and Silhouette metrics, cell patterns were categorized using Nonnegative Matrix Factorization (NMF) method. **F** Bubble plot of receptor-ligand pairs among distinct cell subpopulations. **G** Network localization and functional identification of cell types involved in the PTN and MK signaling pathway. **H** Contribution analysis of key receptor-ligand pairs in the PTN and MK signaling pathway

the early stages of tumor development, dysfunction in the nervous and immune systems may create opportunities for tumor growth to persist [18]. As tumors progress, cytotoxic T cells may become exhausted, while the nervous system provides pathways and structural support for cancer dissemination [19, 20]. These interactions can result in uncontrolled tumor expansion. The nervous system processes and transmits the immune status of the TME to the brain, which then integrates this information and responds back to the TME, creating a comprehensive neural circuit [7, 21, 22].

GABA serves as the primary inhibitory neurotransmitter in the central nervous system, and its deficiency is linked to a range of neurological disorders [23–25]. Research has demonstrated that GABA can regulate various tumor types. For instance, Li et al. found that GABA directly binds to and stabilizes β-catenin, activating Wnt/β-catenin signaling and enhancing metastasis in

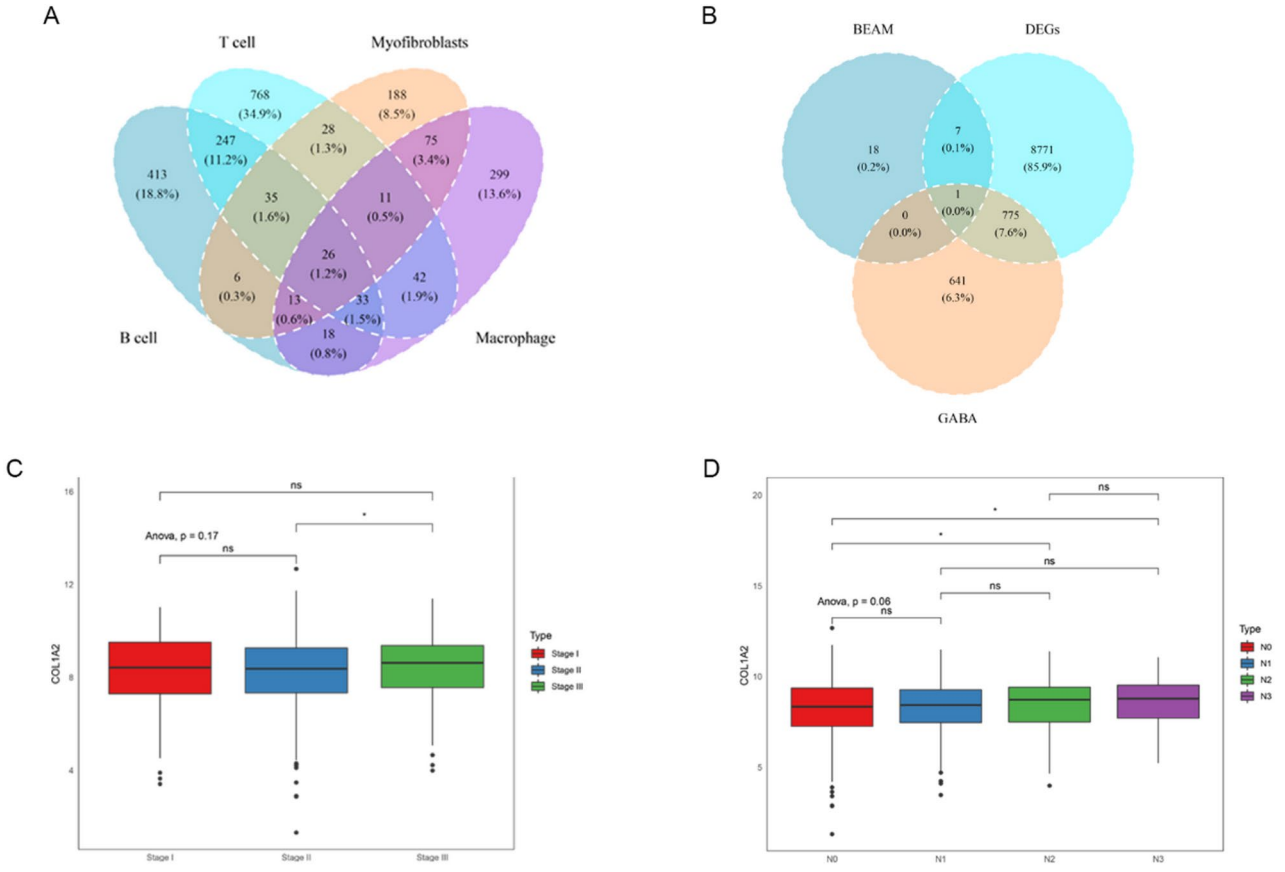

Fig. 7 Acquisition of target genes and clinical analysis. **A** Venn plot based on the BEAM analysis of distinct cell types. **B** Venn plot based on DEGs from bulk RNA-seq, GABA-related genes, and DEGs from BEAM analysis (**A**). **C** The different expression levels of COL1A2 among distinct tumor stage levels. **D** The different expression levels of COL1A2 among distinct T categories

HCC [26]. Dahn et al. suggested that GABA exhibits pro-metastatic properties in breast cancer [27]. Furthermore, Xie et al. identified GABA as crucial in the development of brain metastasis in NSCLC by activating the NF-κB pathway through the FOXA2/ABAT/GABA axis [28]. Li et al. also demonstrated that GPT2 promotes breast cancer metastasis via upregulated GABA activation of the GABAAR-PKC-CREB signaling pathway [29]. However, the potential oncogenic effects of GABA on specific immune cell subpopulations and its regulatory networks remain poorly understood.

Our study aims to systematically explore the cell types present in the TIME in GABA-mediated breast cancer and to identify diverse cell-cell interactions among GABA-associated TIME clusters at both the bulk RNA-seq and scRNA-seq levels. This research seeks to provide a comprehensive understanding of the neuro-immune mechanisms influencing the progression of breast cancer.

The TIME encompasses immunological components that shape tumor development across both dynamic temporal and spatial dimensions, as well as sensitivity to treatment [30]. The cellular composition and the accessibility of immune cells within the TIME exhibit significant heterogeneity across different breast cancer subtypes and among patients [31]. To investigate this heterogeneity, researchers have performed scRNA-seq analyses on $CD45^+$ immune cells from tumor samples of breast cancer patients, as well as matched normal breast tissue, peripheral blood, and lymph node [32]. They identified distinct T cell phenotypes in the blood and lymph nodes compared to those in breast tissue. Additionally, T and myeloid lineage cells exhibited increased phenotypic heterogeneity and expanded cell populations within the tumor. Notably, certain activated macrophage clusters were found to be specific to the tumor environment. The activation state of T cells appears to exist along a continuous gradient rather than being confined to discrete states, as has been traditionally believed. While T cell receptor (TCR) diversity significantly influences T cell phenotypic diversity, it is not the sole determining factor. In this study, we identified 3 distinct T subpopulations and 2 macrophage subclusters modulated by GABA, utilizing an NMF algorithm. Pseudotime analysis of T cells and macrophages revealed that these components exhibited remarkable continuity, essentially representing a single, continuous trajectory (Figs. 3A and 4A). This finding

suggests that the conventional classification of T cell into a limited number of discrete differentiation subtypes may oversimplify the phenotypic complexity of tissue-resident T cell populations. Furthermore, the activation of macrophages in the TME does not conform to the traditional polarization model.

Normal fibroblasts typically suppress tumor formation, whereas cancer-associated fibroblasts (CAFs) facilitate tumor phenotypes, including the proliferation and invasion of tumor cells, inflammation, angiogenesis, and extracellular matrix (ECM) remodeling [33–35]. In breast cancer, αSMA^{+} myofibroblasts are known to promote tumor growth and angiogenesis, serving as predictors of disease recurrence in humans [36, 37]. Costa et al. identified 2 myofibroblast subclusters with high expression of aSMA (CAF-S1 and CAF-S5), and noted that both subsets were preferentially found in tumors. CAF-S1 cells, in particular, attract and retain $CD4^{+}CD25^{+}$ T cells, enhancing T lymphocyte survival and promoting their differentiation into $CD25^{High}FOXP3^{High}$ cells, which contribute to immunosuppression [38]. In our study, we identified 3 myofibroblast subclusters based on GABA-related genes using the NMF algorithm, all of which were exclusively detected in primary tumor samples. The intercellular communication networks indicated that these 3 myofibroblast subclusters extensively interacted with immune cells, including B cells, T cells, and macrophages, through the APP-CD74, CXCL12-CXCR4, and MDK/PTN-NCL axis. Chen et al. reported that APP–CD74 interactions were significantly enhanced between malignant subclusters and 14 types of immune cells, promoting immunosuppression and tumor progression in testicular cancer [39]. Ma et al. found that the APP-CD74 axis exhibited the highest levels of communication between glioblastoma multiforme (GBM) tumor cells and tumor-associated macrophages (TAMs), with both APP and CD74 expression levels corelating with poorer patient outcomes [40]. The CXCL12-CXCR4 axis is a critical signaling pathway involved in breast cancer metastasis [41, 42]. Timperi et al. reported that CAFs interacted with macrophages via the CXCL12-CXCR4 axis, mediating immune suppression in breast cancer [43]. Duan et al. found that FAP^{+} CAFs promoted the proliferation and migration of esophageal squamous carcinoma cells while inhibiting $CD8^{+}$ T cells cytokine secretion [44]. Liu et al. identified that fibroblasts in muscle-invasive bladder cancer (MIBC) patients may attract $CXCR4^{+}$ T cells into the immune microenvironment through CXCL12 chemotaxis [45]. Zhang et al. demonstrated that CAFs induce epithelial-mesenchymal transition (EMT) in ovarian cancer through the CXCL12-CXCR4 axis [41]. Our hallmark analysis indicated that Myo-C1 cells were significantly enriched in pathways associated with EMT. Moreover, MDK-NCL interactions have been linked to the immune environment and tumor progression. MDK has been implicated in reconstructing an immunosuppressive environment in melanoma and gallbladder cancer [46, 47]. Fu et al. showed that MDK-NCL activity suppresses immune cell infiltration and activity, contributing to immune evasion in lung adenocarcinoma (LUAD) [48]. The pronounced APP-CD74, CXCL12-CXCR4, and MDK/PTN-NCL communication signals between myofibroblasts and immune cells observed in our data, combined with findings from previous studies, provide strong evidence to hypothesize that GABA may foster immunosuppression by regulating interactions between myofibroblasts and immune cells via the APP-CD74 axis, thereby promoting breast cancer metastasis.

To explore cell-specific gene regulatory networks in breast cancer, we conducted an analysis of TFs at the single-cell level. Distinctive gene features of TFs were observed in macrophage and myofibroblast subtypes, including TAF1, TAF7, EHF and ELF3 in the M1 macrophage subtype, and TAF1 in Myo_C1 myofibroblast subtype. Wei et al. found that EHF promotes liver cancer metastasis by meditating IL-6 secretion through the transcription regulation of KDM2B in TAMs [49]. TAF7 and TAF1 have also been shown to influence immune responses by regulating the transcription of MHC class I and II molecules [50, 51]. Xu et al. reported that ELF3 is highly expressed in ovarian cancer (OC) tissues and is significantly associated with poor overall survival (OS) and disease-specific survival (DSS) in OC patients. ELF3 was further linked to the presence of immune infiltrating cells [52]. Liu et al. demonstrated that ELF3 promotes the expression of mucin-16 (MUC16), facilitating glycolysis-mediated immune escape in nasopharyngeal carcinoma (NPC) cells [53]. These findings suggest that macrophages and myofibroblasts in breast cancer may activate these TFs to establish an immunosuppressive microenvironment, thus promoting breast cancer metastasis. Consequently, we hypothesize that GABA-mediated interactions between macrophage and myofibroblast subtypes may contribute to the immunosuppressive landscape surrounding tumor cells, facilitating breast cancer metastasis. This research provides innovative and comprehensive insights into potential therapeutic targets within the context of GABA-related genes and immune cell modulation, which play critical roles in regulating breast cancer development.

T cells constitute a significant portion of the immune infiltrate in breast cancer, serving as a crucial line of defense against cancer cells [54]. The level of T cell infiltration and their functional status directly influence tumor progression and treatment outcomes [54, 55]. Numerous studies have demonstrated that GABA plays a role in regulating the differentiation and functional activity of T cell subsets, thereby affecting the overall

immune response. Huang et al. demonstrated that cancer cell-derived GABA activates the GABAB receptor, which inhibits GSK-3β activity, This inhibition leads to enhanced β-catenin signaling, resulting in increased tumor cell proliferation and reduced intratumoral infiltration of $CD8^+$ T cells [10]. Zhou et al. reported that PMVK enhances GABA synthesis and facilitates its conversion into 4-Ac-GABA, which activates the GABAAR on $CD8^+$ T cells, thereby inhibiting $CD8^+$ T cell activation and the anti-tumor response [56]. In our analysis, we identified 3 T cell subclusters based on GABA-related genes and the NMF algorithm. We observed extensive interactions between T cell subclusters and myofibroblasts. Furthermore, we found that $CD4^+$ Tprol cells exhibit a distinct KDM5A gene signature, as revealed by TFs analysis. Li et al. found that KDM5A is highly expressed in TNBC, and patients with elevated levels of KDM5A have poor overall survival. KDM5A promotes the demethylation of histone H3K4me3, leading to the downregulation of p16 expression, which contributes to tumorigenesis and metastasis in TNBC [57]. The study of Liu et al. revealed that KDM5A drives Th2 polarization by selectively demethylating H3K4me3 at the IL4 promoter, thereby enhancing IL-4 transcription in $CD4^+$ T cells [58].

B cells are a significant component of tumor-infiltrating leukocytes and play a crucial role in tumor progression and prognosis [59]. They are involved in presenting cancer antigens to T cells, regulating T cell function through cytokine secretion, forming tertiary lymphoid structures (TLSs) in or around tumors, and producing antibodies [60, 61]. In our study, we identified 6 B cell subclusters based on GABA-related genes and the NMF algorithm, and we discovered a unique gene signature associated with XBP1 in the B_C4 subcluster through transcription factor analysis. XBP1, a transcription factor belonging to the CREB/ATF family, is predominantly expressed in plasma cells and plays a critical role in regulating plasma cell differentiation [62]. Yang et al. [63] and Fitzsimons et al. [64] have characterized phenotypically distinct B cell subtypes using scRNA-seq across various cancers. They identified a B cell subcluster that exhibited high expression of XBP1, which serves as a marker for plasma cells and is associated with the differentiation of antibody-secreting cells. Previous studies have demonstrated that antibodies produced by plasma cells can mediate antitumor activity, and elevated levels of plasma cells have been correlated with favorable outcomes in breast cancer [65], nasopharyngeal carcinoma [66], and lung adenocarcinoma [67]. In our analysis, the pseudotime trajectories of GABA-mediated B cell subpopulations indicated that B_C4 was predominantly situated in the terminal state, and we observed a significantly reduced proportion of B_C4 in metastatic samples compared to primary tumor samples. This suggests that GABA may contribute to an immunosuppressive microenvironment by inhibiting plasma cells differentiation, thereby facilitating breast cancer metastasis.

Our study has several limitations. First, with only one sample per condition (primary, NLN, PLN), the study lacks biological replicates; therefore, all comparisons of cell subpopulation proportions are descriptive and hypothesis-generating rather than statistically conclusive. Potential effects of tissue dissociation and sampling bias cannot be ruled out. Second, we did not conduct further subtyping of breast cancer, which may obscure subtype-specific differences in the interactions between GABA and TIME components. Additionally, the limited availability of comprehensive clinical information from public datasets has constrained our ability to investigate these differences further. Third, additional experimental validation, both in vitro and in vivo, is necessary to provide more robust support for our conclusions. Nevertheless, the consistency of key findings in an independent scRNA-seq cohort (GSE180286) strengthens the validity of our observations. Furthermore, due to the inherent limitations of public datasets, we were unable to incorporate clinical variables or spatial information regarding the immune microenvironment, which could offer deeper insights into the clinical relevance of our findings. Further studies should aim to integrate experimental validation, subtype-specific analysis, and spatial transcriptomics to address these limitations and enhance the translational value of our research.

In summary, our findings provide a first comprehensive single-cell atlas of GABA-associated TIME cell types in breast cancer metastasis, offering novel insights into the potential role of GABA in breast cancer progression and suggesting implications for personalized treatment strategies. This work lays the groundwork for further investigation into how GABA may influence the tumor microenvironment.

Supplementary Information

The online version contains supplementary material available at https://doi.org/10.1186/s13058-026-02268-x.

Supplementary Material 1.

Supplementary Material 2.

Acknowledgements
Not applicable.

Author contributions
LNT conceived the study, performed the data analysis, the manuscript, and revised the article. All the authors have read and approved the final version of the manuscript.

Funding
The author(s) declare that financial support was received for the research and/or publication of this article. This study was supported by the Natural Science

Foundation of Henan Province (232300420243, 262300422310), Research Fund of Zhengzhou Central Hospital (SR-0048).

Data availability
All data used in this study were sourced from the public databases online or may be made available from the corresponding author upon reasonable request.

Declarations

Ethics approval and consent to participate
Not applicable.

Consent for publication
Not applicable.

Competing interests
The authors declare no competing interests.

Author details
[1]Institute of Trauma and Metabolism, Zhengzhou Central Hospital Affiliated to Zhengzhou University, Zhengzhou 450001, China

Received: 4 December 2025 / Accepted: 22 March 2026
Published online: 31 March 2026

References

1. Park M, Kim D, Ko S, Kim A, Mo K, Yoon H. Breast cancer metastasis: mechanisms and therapeutic implications. Int J Mol Sci. 2022;23(12):6806.
2. Peng C, Xu Y, Wu J, Wu D, Zhou L, Xia X. TME-Related Biomimetic Strategies Against Cancer. Int J Nanomed. 2024;19:109–35.
3. Liu Y, He S, Wang XL, Peng W, Chen QY, Chi DM, et al. Tumour heterogeneity and intercellular networks of nasopharyngeal carcinoma at single cell resolution. Nat Commun. 2021;12:741.
4. Monteran L, Ershaid N, Doron H, Zait Y, Scharff Y, Ben-Yosef S, et al. Chemotherapy-induced complement signaling modulates immunosuppression and metastatic relapse in breast cancer. Nat Commun. 2022;13:5797.
5. Zeng W, Zhang R, Huang P, Chen M, Chen H, Zeng X, et al. Ferroptotic Neutrophils Induce Immunosuppression and Chemoresistance in Breast Cancer. Cancer Res. 2025;85:477–96.
6. Whiteley AE, Ma D, Wang L, Yu SY, Yin C, Price TT, et al. Breast cancer exploits neural signaling pathways for bone-to-meninges metastasis. Science. 2024;384:eadh5548.
7. Amit M, Eichwald T, Roger A, Anderson J, Chang A, Vermeer PD, et al. Neuroimmune cross-talk in cancer. Nat Rev Cancer. 2025;25:573–89.
8. Padmanaban V, Keller I, Seltzer ES, Ostendorf BN, Kerner Z, Tavazoie SF. Neuronal substance P drives metastasis through an extracellular RNA-TLR7 axis. Nature. 2024;633:207–15.
9. Ngo DH, Vo TS. An updated review on pharmaceutical properties of gamma-aminobutyric acid. Molecules. 2019;24(15):2678.
10. Huang D, Wang Y, Thompson JW, Yin T, Alexander PB, Qin D, et al. Cancer-cell-derived GABA promotes beta-catenin-mediated tumour growth and immunosuppression. Nat Cell Biol. 2022;24:230–41.
11. Zhang B, Vogelzang A, Miyajima M, Sugiura Y, Wu Y, Chamoto K, et al. B cell-derived GABA elicits IL-10(+) macrophages to limit anti-tumour immunity. Nature. 2021;599:471–6.
12. Dong Y, Wang G, Nie D, Xu Y, Bai X, Lu C, et al. Tumor-derived GABA promotes lung cancer progression by influencing TAMs polarization and neovascularization. Int Immunopharmacol. 2024;126:111217.
13. El-Tanani M, Rabbani SA, Babiker R, Rangraze I, Kapre S, Palakurthi SS, et al. Unraveling the tumor microenvironment: Insights into cancer metastasis and therapeutic strategies. Cancer Lett. 2024;591:216894.
14. de Visser KE, Joyce JA. The evolving tumor microenvironment: From cancer initiation to metastatic outgrowth. Cancer Cell. 2023;41:374–403.
15. Liang S, Hess J. Tumor neurobiology in the pathogenesis and therapy of head and neck cancer. Cells. 2024;13(3):256.
16. Xu Q, Cao Y, Kong F, Liu J, Chen X, Zhao Y, et al. Multiple cancer cell types release LIF and Gal3 to hijack neural signals. Cell Res. 2024;34:345–54.
17. Winkler F, Venkatesh HS, Amit M, Batchelor T, Demir IE, Deneen B, et al. Cancer neuroscience: State of the field, emerging directions. Cell. 2023;186:1689–707.
18. Pu T, Sun J, Ren G, Li H. Neuro-immune crosstalk in cancer: mechanisms and therapeutic implications. Signal Transduct Target Ther. 2025;10:176.
19. Chow A, Perica K, Klebanoff CA, Wolchok JD. Clinical implications of T cell exhaustion for cancer immunotherapy. Nat Rev Clin Oncol. 2022;19:775–90.
20. Wang Q, Qin Y, Li B. CD8(+) T cell exhaustion and cancer immunotherapy. Cancer Lett. 2023;559:216043.
21. Udit S, Blake K, Chiu IM. Somatosensory and autonomic neuronal regulation of the immune response. Nat Rev Neurosci. 2022;23:157–71.
22. Karschnia P, Nelson TA, Dietrich J. Mechanisms and treatment of cancer therapy-induced peripheral and central neurotoxicity. Nat Rev Cancer. 2025;25(12):887–909.
23. Cherubini E, Di Cristo G, Avoli M. Dysregulation of GABAergic Signaling in Neurodevelomental Disorders: Targeting Cation-Chloride Co-transporters to Re-establish a Proper E/I Balance. Front Cell Neurosci. 2021;15:813441.
24. Yuan H, Low CM, Moody OA, Jenkins A, Traynelis SF. Ionotropic GABA and Glutamate Receptor Mutations and Human Neurologic Diseases. Mol Pharmacol. 2015;88:203–17.
25. Fontes MAP, Vaz GC, Cardoso TZD, de Oliveira MF, Campagnole-Santos MJ, Dos Santos RAS, et al. GABA-containing liposomes: neuroscience applications and translational perspectives for targeting neurological diseases. Nanomedicine. 2018;14:781–8.
26. Li L, Kang Y, Cheng R, Liu F, Wu F, Liu Z et al. The de novo synthesis of GABA and its gene regulatory function control hepatocellular carcinoma metastasis. Dev Cell 2025;60:1053–1069 e1056.
27. Dahn ML, Walsh HR, Dean CA, Giacomantonio MA, Fernando W, Murphy JP, et al. Metabolite profiling reveals a connection between aldehyde dehydrogenase 1A3 and GABA metabolism in breast cancer metastasis. Metabolomics. 2022;18:9.
28. Xie M, Qin H, Liu L, Wu J, Zhao Z, Zhao Y, et al. GABA regulates metabolic reprogramming to mediate the development of brain metastasis in non-small cell lung cancer. J Exp Clin Cancer Res. 2025;44:61.
29. Li N, Xu X, Liu D, Gao J, Gao Y, Wu X, et al. The delta subunit of the GABA(A) receptor is necessary for the GPT2-promoted breast cancer metastasis. Theranostics. 2023;13:1355–69.
30. Zhou Z, Wang J, Wang J, Yang S, Wang R, Zhang G, et al. Deciphering the tumor immune microenvironment from a multidimensional omics perspective: insight into next-generation CAR-T cell immunotherapy and beyond. Mol Cancer. 2024;23:131.
31. Harris MA, Savas P, Virassamy B, O'Malley MMR, Kay J, Mueller SN, et al. Towards targeting the breast cancer immune microenvironment. Nat Rev Cancer. 2024;24:554–77.
32. Azizi E, Carr AJ, Plitas G, Cornish AE, Konopacki C, Prabhakaran S, et al. Single-Cell Map of Diverse Immune Phenotypes in the Breast Tumor Microenvironment. Cell. 2018;174:1293–308. e1236.
33. Gentric G, Mieulet V, Mechta-Grigoriou F. Heterogeneity in Cancer Metabolism: New Concepts in an Old Field. Antioxid Redox Signal. 2017;26:462–85.
34. Gascard P, Tlsty TD. Carcinoma-associated fibroblasts: orchestrating the composition of malignancy. Genes Dev. 2016;30:1002–19.
35. Costa A, Scholer-Dahirel A, Mechta-Grigoriou F. The role of reactive oxygen species and metabolism on cancer cells and their microenvironment. Semin Cancer Biol. 2014;25:23–32.
36. Toullec A, Gerald D, Despouy G, Bourachot B, Cardon M, Lefort S, et al. Oxidative stress promotes myofibroblast differentiation and tumour spreading. EMBO Mol Med. 2010;2:211–30.
37. Benyahia Z, Dussault N, Cayol M, Sigaud R, Berenguer-Daize C, Delfino C, et al. Stromal fibroblasts present in breast carcinomas promote tumor growth and angiogenesis through adrenomedullin secretion. Oncotarget. 2017;8:15744–62.
38. Costa A, Kieffer Y, Scholer-Dahirel A, Pelon F, Bourachot B, Cardon M et al. Fibroblast heterogeneity and immunosuppressive environment in human breast cancer. Cancer Cell. 2018;33:463–479 e410.
39. Chen G, Wang W, Wei X, Chen Y, Peng L, Qu R, et al. Single-cell transcriptomic analysis reveals that the APP-CD74 axis promotes immunosuppression and progression of testicular tumors. J Pathol. 2024;264:250–69.
40. Ma C, Chen J, Ji J, Zheng Y, Liu Y, Wang J, et al. Therapeutic modulation of APP-CD74 axis can activate phagocytosis of TAMs in GBM. Biochim Biophys Acta Mol Basis Dis. 2024;1870:167449.
41. Zhou W, Guo S, Liu M, Burow ME, Wang G. Targeting CXCL12/CXCR4 Axis in Tumor Immunotherapy. Curr Med Chem. 2019;26:3026–41.

42. Wani N, Nasser MW, Ahirwar DK, Zhao H, Miao Z, Shilo K, et al. C-X-C motif chemokine 12/C-X-C chemokine receptor type 7 signaling regulates breast cancer growth and metastasis by modulating the tumor microenvironment. Breast Cancer Res. 2014;16:R54.
43. Timperi E, Gueguen P, Molgora M, Magagna I, Kieffer Y, Lopez-Lastra S, et al. Lipid-Associated Macrophages Are Induced by Cancer-Associated Fibroblasts and Mediate Immune Suppression in Breast Cancer. Cancer Res. 2022;82:3291–306.
44. Duan L, Cao S, Zhao F, Du X, Gao Z, Wang X, et al. Effects of FAP+ fibroblasts on cell proliferation migration and immunoregulation of esophageal squamous carcinoma cells through the CXCL12/CXCR4 axis. Mol Cell Biochem. 2025;480:3841–55.
45. Liu Z, Mao X, Xie Y, Yan Y, Wang X, Mi J, et al. Single-cell RNA sequencing reveals a fibroblast gene signature that promotes T-cell infiltration in muscle-invasive bladder cancer. Commun Biol. 2025;8:696.
46. Zhang Y, Zuo C, Liu L, Hu Y, Yang B, Qiu S, et al. Single-cell RNA-sequencing atlas reveals an MDK-dependent immunosuppressive environment in ErbB pathway-mutated gallbladder cancer. J Hepatol. 2021;75:1128–41.
47. Cerezo-Wallis D, Contreras-Alcalde M, Troule K, Catena X, Mucientes C, Calvo TG, et al. Midkine rewires the melanoma microenvironment toward a tolerogenic and immune-resistant state. Nat Med. 2020;26:1865–77.
48. Fu Y, Li S, Zhao Y, Zhang X, Mao X, Xu R. Integrative single-cell and spatial transcriptomics analysis reveals MDK-NCL pathway's role in shaping the immunosuppressive environment of lung adenocarcinoma. Front Immunol. 2025;16:1546382.
49. Wei S, Zhao S, Yang W, Zhou J, Xu G, Zhang C, et al. EHF promotes liver cancer progression by meditating IL-6 secretion through transcription regulation of KDM2B in TAMs. Cell Signal. 2025;129:111670.
50. Devaiah BN, Lu H, Gegonne A, Sercan Z, Zhang H, Clifford RJ, et al. Novel functions for TAF7, a regulator of TAF1-independent transcription. J Biol Chem. 2010;285:38772–80.
51. Soe KC, Devaiah BN, Singer DS. Transcriptional coactivator CIITA, a functional homolog of TAF1, has kinase activity. Biochim Biophys Acta. 2013;1829:1184–90.
52. Xu H, Wang H, Li G, Jin X, Chen B. The Immune-Related Gene ELF3 is a Novel Biomarker for the Prognosis of Ovarian Cancer. Int J Gen Med. 2021;14:5537–48.
53. Liu Y, Zhou H, Yu Q, Wang Q. Hypomethylation-associated ELF3 helps nasopharyngeal carcinoma to escape immune surveillance via MUC16-mediated glycolytic metabolic reprogramming. Am J Physiol Cell Physiol. 2024;327:C1125–42.
54. Tietscher S, Wagner J, Anzeneder T, Langwieder C, Rees M, Sobottka B, et al. A comprehensive single-cell map of T cell exhaustion-associated immune environments in human breast cancer. Nat Commun. 2023;14:98.
55. Liang H, Huang J, Li H, He W, Ao X, Xie Z, et al. Spatial proximity of CD8(+) T cells to tumor cells predicts neoadjuvant therapy efficacy in breast cancer. NPJ Breast Cancer. 2025;11:13.
56. Zhou X, Chen Z, Yu Y, Li M, Cao Y, Prochownik EV, et al. Increases in 4-Acetaminobutyric Acid Generated by Phosphomevalonate Kinase Suppress CD8(+) T Cell Activation and Allow Tumor Immune Escape. Adv Sci (Weinh). 2024;11:e2403629.
57. Li S, He J, Liao X, He Y, Chen R, Chen J, et al. Fbxo22 inhibits metastasis in triple-negative breast cancer through ubiquitin modification of KDM5A and regulation of H3K4me3 demethylation. Cell Biol Toxicol. 2023;39:1641–55.
58. Liu J, Liu Z, Geng X, Wu Y, Mo L, Liao Y et al. KDM5A: a master epigenetic regulator of Th2 immunity and allergic disease pathogenesis. Immunology. 2025.
59. Wei Y, Huang CX, Xiao X, Chen DP, Shan H, He H, et al. B cell heterogeneity, plasticity, and functional diversity in cancer microenvironments. Oncogene. 2021;40:4737–45.
60. de Gruijter NM, Jebson B, Rosser EC. Cytokine production by human B cells: role in health and autoimmune disease. Clin Exp Immunol. 2022;210:253–62.
61. Rastogi I, Jeon D, Moseman JE, Muralidhar A, Potluri HK, McNeel DG. Role of B cells as antigen presenting cells. Front Immunol. 2022;13:954936.
62. Shaffer AL, Shapiro-Shelef M, Iwakoshi NN, Lee AH, Qian SB, Zhao H, et al. XBP1, downstream of Blimp-1, expands the secretory apparatus and other organelles, and increases protein synthesis in plasma cell differentiation. Immunity. 2004;21:81–93.
63. Yang Y, Chen X, Pan J, Ning H, Zhang Y, Bo Y et al. Pan-cancer single-cell dissection reveals phenotypically distinct B cell subtypes. Cell. 2024;187:4790–4811 e4722.
64. Fitzsimons E, Qian D, Enica A, Thakkar K, Augustine M, Gamble S, et al. A pan-cancer single-cell RNA-seq atlas of intratumoral B cells. Cancer Cell. 2024;42:1784–97. e1784.
65. Sakaguchi A, Horimoto Y, Onagi H, Ikarashi D, Nakayama T, Nakatsura T, et al. Plasma cell infiltration and treatment effect in breast cancer patients treated with neoadjuvant chemotherapy. Breast Cancer Res. 2021;23:99.
66. Liu Y, Ye SY, He S, Chi DM, Wang XZ, Wen YF, et al. Single-cell and spatial transcriptome analyses reveal tertiary lymphoid structures linked to tumour progression and immunotherapy response in nasopharyngeal carcinoma. Nat Commun. 2024;15:7713.
67. Hao D, Han G, Sinjab A, Gomez-Bolanos LI, Lazcano R, Serrano A, et al. The Single-Cell Immunogenomic Landscape of B and Plasma Cells in Early-Stage Lung Adenocarcinoma. Cancer Discov. 2022;12:2626–45.

Publisher's Note

Springer Nature remains neutral with regard to jurisdictional claims in published maps and institutional affiliations.